Storm-Relative Flow and its Relationship to Low-Level Vorticity in Simulated Storms

Cody Kirkpatrick
University of Alabama in Huntsville

Eugene W. McCaul, Jr.
Universities Space Research Association

1. INTRODUCTION

There is substantial evidence documenting the effects of environmental wind shear on storm morphology. Prior numerical modeling studies have explored the sensitivity of storm evolution to systematic changes in the shear profile (e.g., Weisman and Klemp 1982, 1984; Droegemeier et al. 1993; Adlerman and Droegemeier 2005). Increasing the ambient low-level shear leads to stronger mesocyclones (McCaul and Weisman 2001), and mesocyclones are apparently strongest when "the greatest shears are confined to the shallowest depths" (Adlerman and Droegemeier 2005, p. 3619). Certain kinematic parameters can discriminate between supercell and nonsupercell environments (e.g., Rasmussen and Blanchard 1998), and between short-lived and long-lived supercell storms (Bunkers et al. 2006). Thompson et al. (2003) studied model-based proximity soundings, finding that the 0–6 km vector shear magnitude shows utility in discriminating between tornadic and nontornadic supercells, with the 0-1 km vector shear magnitude further discriminating between "significantly" tornadic (F2 or greater damage) and "weakly" tornadic (F0 or F1 damage) storms. Storm motions are also driven to a large degree by the environmental wind profile (e.g., Bunkers et al. 2000; Kirkpatrick et al. 2007).

With a fixed storm motion, increasing the low-level shear corresponds to an increase storm-relative helicity (SRH; Davies-Jones et al. 1990), since there is a strong correlation between low-level winds and SRH ($r = 0.7$ in a set of 425 supercell proximity soundings provided by M. Bunkers; see also Bunkers et al. 2006). Kerr and Darkow (1996) specifically examined the effects of storm-relative (SR) winds on tornadic storms, finding stronger SR low-level flow in cases where violent tornadoes occurred. Middle-

and upper-level SR winds also play an important role by influencing a storm's precipitation distribution (e.g., Rasmussen and Straka 1998). The effect of SR winds on storm organization, and specifically on storm low-level vorticity production, is the focus of this paper.

To examine SR winds, we define a "storm inflow–outflow angle," α, which is the angle between the SR low-level (V_{SRL}) and SR upper-level (V_{SRU}) wind vectors (Fig. 1). The low-level flow is assumed to be representative of the storm inflow layer, and is taken to be the mean wind in the 0–1 km layer. The upper-level flow is assumed to be representative of the anvil layer, and is taken to be the average wind from 9–11 km, although this can be varied within limits without significant changes to the results (discussed in section 3).

When the angle α between V_{SRL} and V_{SRU} is approximately 180° (as in Fig. 1), storm inflow trajectories are closely aligned with the baroclinic region on the periphery of the forward-flank downdraft, and many inflow trajectories will pass through this region. In this case, the vorticity that is induced along the forward outflow is purely streamwise, and can then be ingested by the updraft. This can produce a large increase in low-level vertical vorticity. When α is greater than 180° (Fig. 2a and b), storm inflow will be across the precipitation footprint. This causes the updraft to ingest its own rain-cooled outflow, and low-level mesocyclone strength will be inhibited. When α is less than 180° (Fig. 2c and d), inflow trajectories are from ambient, undisturbed air. While this may not cause a *decrease* in low-level mesocyclone strength, a storm in this environment will be unable to take full advantage of the vorticity available along its outflow.

2. DATA

The simulations studied in this paper are part of a 216 simulation subset of the Convection Morphology Parameter Space Study (COMPASS; McCaul and
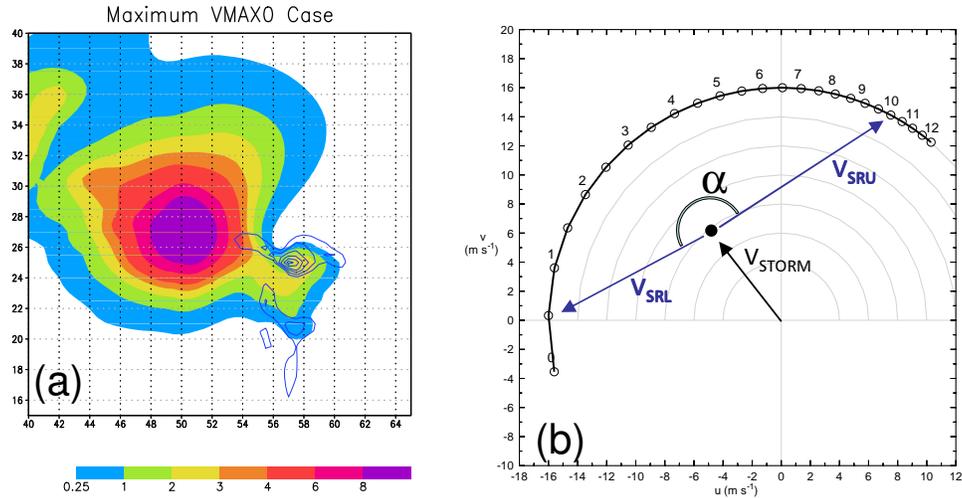
Fig. 1. (a) Simulation output for the experiment with the greatest second-hour mean VMAX0, at a time representative of the mature storm for that simulation. Surface rainwater mixing ratio (g kg^{-1}) is shaded, and vorticity at the lowest model level is contoured (0.005 s^{-1}, beginning at 0.005 s^{-1}). Axes are in km. (b) Hodograph representation of the wind profile used in (a), with storm motion shown as V$_{\text{STORM}}$. SR lower- (V$_{\text{SRL}}$) and upper-level (V$_{\text{SRU}}$) wind vectors are shown in blue. Hodograph points are at 500 m increments, with every other point labeled in km.
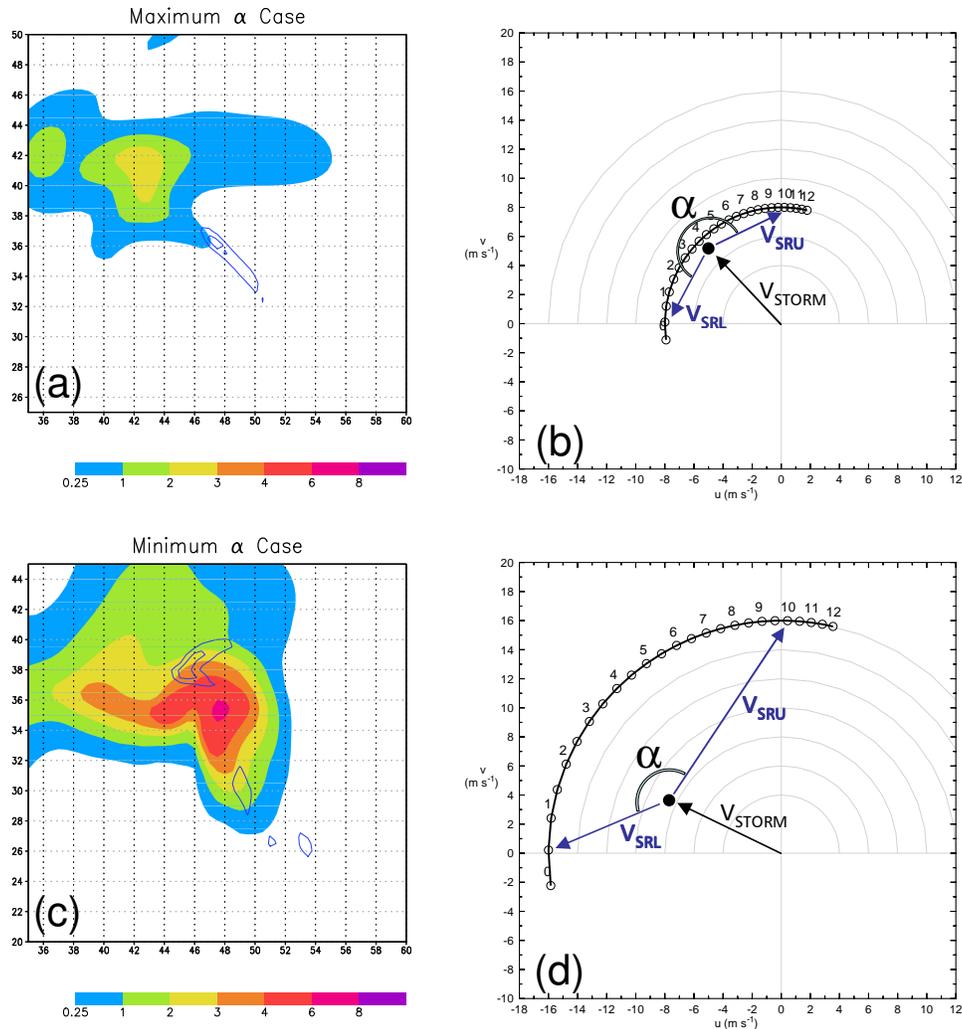

Fig. 2. As in Fig. 1, but for two non-optimal cases for α. In (a) and (b), α is much greater than 180°; in (c) and (d), α is much less than 180°.

Table 1. Parameter choices available for COMPASS initial
soundings.

Parameter	Possible Values
Bulk CAPE	800, 2000, 3200 J kg^{-1}
Semicircular hodo. radius	8, 12, 16 m s^{-1}
Shape of buoyancy profile	Two choices per CAPE
Shape of shear profile	Two choices per CAPE
LCL-LFC configuration	0.5-0.5, 0.5-1.6, 1.6-1.6 km
Precipitable water (PW)	Roughly 30 or 60 mm
RH above LFC	Constant, 90%

Cohen 2002), and are performed with the Regional
Atmospheric Modeling System (RAMS) version 3b,
with some modifications (see McCaul et al. 2005).
Eight variables define the COMPASS parameter
space (Table 1). The two choices of shear profile
shape correspond to the buoyancy profile shape
parameter choices, which are constrained by CAPE.
At each CAPE value, the buoyancy profile shapes
are chosen so as to avoid the creation of lapse
rates greater than dry adiabatic. Storms are ini-
tialized using an LCL-conserving thermal bubble in
an otherwise homogeneous 75 × 75 km horizontal
domain. The horizontal grid spacing is 500 m, and
the vertical mesh is stretched, with 250 m resolution
at the surface and 750 m resolution near the fixed
tropopause (14.5 km). Further model specifications
are described in McCaul et al. (2005). To simplify
interpretation of the results, the parameters that
determine the size distributions and concentrations
of ice and water species are held constant. Although
our horizontal spacing is insufficient to resolve tor-
nado circulations explicitly, we focus here on general
low-level mesocyclone intensity, and 500 m horizon-
tal resolution should be sufficient to resolve storm
mesocyclones.

Of the 216 simulations considered here, 139 pro-
duce a "persistent," discrete right-moving storm
with a mean updraft velocity of at least 10 m s^{-1}
during the second hour. The maximum mid-level
vertical velocity (WMAX) and maximum vertical
vorticity at the lowest model level (126 m AGL;
VMAX0) averaged over the second hour (at 5 min
intervals) are calculated for each storm. As in Kirk-
patrick et al. (2007), the 139 simulated storms are
binned into 72 "supercells" and 67 "nonsupercells."
A storm is considered a supercell if its mean mid-

level vorticity in the second hour is at least 0.01 s^{-1},
and its mean linear updraft-vorticity correlation co-
efficient is 0.4 or greater over the same time period.
Any storm not meeting both these criteria is con-
sidered a nonsupercell. These conditions admittedly
are arbitrary, and some marginal supercell storms
with strong rotation but low correlation coefficients
may be excluded as a result. However, nonsupercell
storms with strong rotation have been documented
(Wakimoto and Wilson 1989).

3. RESULTS

Mean second-hour VMAX0 values binned by α
are shown in Fig. 3. In the simulation set, the
experiment with the greatest VMAX0 has $\alpha =
178°$, and generally, VMAX0 is maximized when
α is near 180°. Both the extreme and median
values decrease rapidly as α increases above 180°.
In these latter environments, storm motions are
closer to the hodograph, the inflow is disturbed
by precipitation, and updrafts are also generally
much weaker (WMAX, Fig. 4). When α is less
than 180°, defining a trend in the median VMAX0
is difficult because the simulation set contains few
storms in these environments. However, there is a
decreasing trend in the VMAX0 maxima between
bins where $\alpha < 180°$. This decline in VMAX0 at
lower α is concomitant with a dramatic *increase*
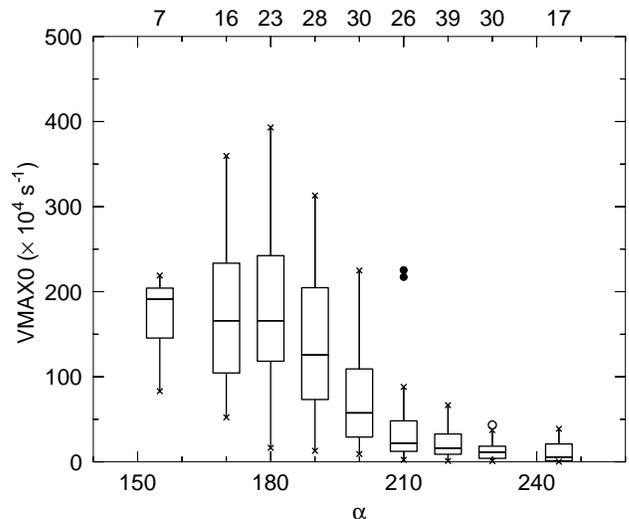in WMAX, and our strongest updrafts occur in

Fig. 3. Standard box plots of VMAX0 ($\times 10^4$ s^{-1}) as a
function of inflow-outflow angle, α. The middle seven bins
include all storms within a 10° range of α (e.g., 165-175°, 175-
185°, etc.), and the outer left (right) bin includes all storms
with α less than 165° (greater than 235°). The number of
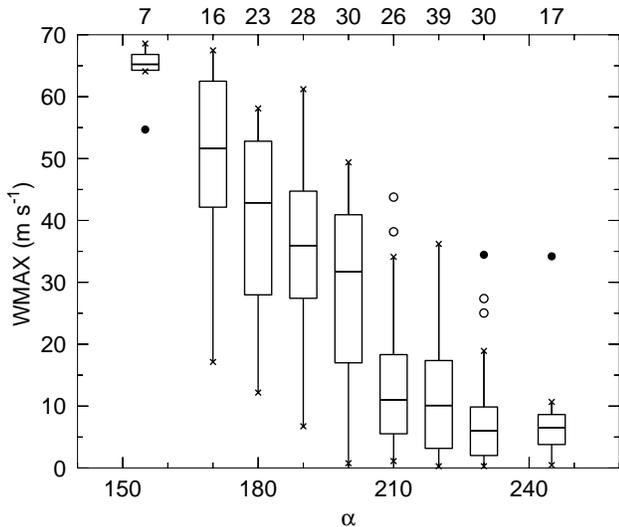storms in each bin is given above the plot; all 216 experiments
are included.

Fig. 4.   As in Fig. 3, for WMAX (m s^{-1}).

Table 2. SR inflow-outflow angle α for the simulation that produces the maximum average second-hour VMAX0 (shown in Fig. 1), as a function of anvil layer choice and whether the simulated motion or its forecast (using B2K) is used.

Anvil Layer	α (V_{STORM})	α (V_{B2K})
9–11 km	179°	170°
10–12 km	185°	176°
12–14 km	194°	186°
10–14 km	190°	181°

storms that have the smallest α and the largest off-hodograph deviate motions (not shown). The large deviate motions likely permit these storms to ingest a greater amount of undisturbed, high-θ_e air, thereby enhancing the buoyant energy available for the updraft.

A scatterplot of the 139 "persistent" storms (Fig. 5) shows that storms with the greatest VMAX0 consist largely of our 3200-CAPE, large hodograph radius simulations, which are conditions generally conducive of strong, rotating updrafts. There are, however, a number of storms with α near 180° that do not produce large VMAX0, and these generally are found in environments with less shear and high Bulk Richardson Numbers, and are thus more prone to more multicell, pulse-like behavior. Thus, knowledge of the value of α may be most useful when the likelihood of supercell convection is increased.

Since *a priori* knowledge of storm motion is not always available, it is useful to explore these results using a storm motion forecast. One popular technique developed by Bunkers et al. (2000, B2K hereafter) will be studied here. B2K was designed using *supercell* proximity soundings, and thus can be used reliably only on the 72 supercell-producing simulations in the dataset. When using B2K, VMAX0 is maximized at approximately 170°, with the highest VMAX0 values again occurring in the range of 150–180° (Fig. 6). There is a tendency for B2K to over-predict deviate motions in our simulation set (as noted by Kirkpatrick et al. 2007), and this is the likely reason for the cluster of supercell storms with low VMAX0 and low α at the left of Fig. 6. These storms do not have weak updrafts (for the

eight supercells with $\alpha < 140°$, WMAX averages 24 m s^{-1}), but do have large differences between their actual motions and the motions forecast by B2K (average error 5.4 m s^{-1}, with all outside B2K's original MAE of 4.1 m s^{-1}).

The effects of varying the anvil layer are summarized in Table 2. Peak α is relatively insensitive to anvil layer choice, varying most (16°) when the layer is changed from the lowest (9–11 km) to highest (12–14 km) layers considered. Since our hodographs are approximately semicircles, variations in α may be more noticeable here than in studies of observed storms and proximity soundings, where the directional variation in upper-level wind is not as pronounced. The choice of anvil layer will also affect the number of simulations in each data bin in Figs. 3 and 4. Table 2 seems to suggest that maximum VMAX0 is realized when α is near 180°, regardless of the choice of anvil layer.

Kerr and Darkow (1996) studied SR winds in 184 tornadic proximity soundings, and α was less than 180° for the mean hodograph in all four of their intensity bins (F0, F1, F2, and F3–F4). All four categories had an α near 140°, with the F2 category having the lowest value (132°).[1] Their study implies that strong storms do exist in environments where α is significantly less than 180°, suggesting that the present research could benefit from expansion to a larger, observational dataset of storms.

4. SUMMARY

The ability of a storm to maximize its low-level vorticity is enhanced when α, the angle between SR-inflow and SR-outflow, is approximately 180°, owing to the greater likelihood that inflow trajectories will experience the increased baroclinity near the

---

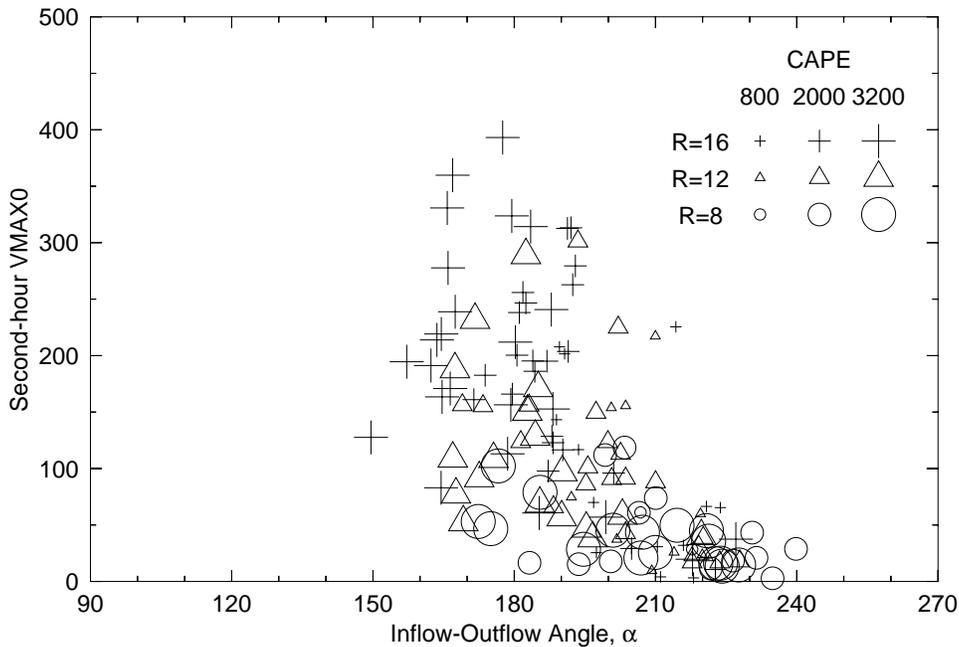[1]Subjectively analyzed from Fig. 9 of Kerr and Darkow (1996).

Fig. 5. Storm inflow–outflow angle, α, in degrees, based on second-hour simulated storm motions, and average second-hour low-level vorticity (VMAX0, $\times 10^4$ s^{-1}). Increasing CAPE is denoted by symbol size, and different hodograph radii (R; in m s^{-1}) are noted by unique symbols. Only the 139 persistent storms (defined in the text) are retained.

storm's forward precipitation region. This relationship is robust to a variety of choices of anvil layer depth and height. The present results describe an aspect of the relationship between storm evolution and the environmental wind profile that has received relatively little attention in the literature. Future observational studies should embrace and consider additional features of the storm-relative wind profile that may help to explain why some strong storms produce low-level mesocyclones and tornadoes, while others do not.

The present work offers a number of opportunities for expanded study. A preliminary analysis of parcel trajectories for the simulation in Fig. 1 finds that the α of actual parcels is in fact near 180°. Further trajectory calculations for other simulations (with varying values of expected α, calculated from the bulk wind profile) are warranted. Relationships may also exist between VMAX0 and storm motion, especially within the 5-min model output fields available for analysis. Some groups of simulations bearing similar environmental conditions should be evaluated separately, since the "bulk" statistical approach used herein can sometimes mask important trends when many cases from many environmental regimes are combined (c.f. Kirkpatrick et al. 2006). An objective definition of the anvil and inflow layers (similar to calculations of, e.g., "effective shear;" Thompson et al. 2007) as a function of environment

might also prove useful in better defining α and its impacts. Additional LES-scale simulations of certain cases having large cyclonic VMAX0 may yield insight into the ways mesocyclone-scale vorticity leads to tornadogenesis.

Project Website

For additional information, visit our project website at http://space.hsv.usra.edu/COMPASS/.

References

Adlerman, E. J. and K. K. Droegemeier, 2005: The dependence of numerically simulated cyclic mesocyclogenesis upon environmental vertical wind shear. *Mon. Wea. Rev.*, **133**, 3595–3623.

Bunkers, M. J., J. S. Johnson, L. J. Czepyha, J. M. Grzywacz, B. A. Klimowski, and M. R. Hjelmfelt, 2006: An observational examination of long-lived supercells. Part II: Environmental conditions and forecasting. *Wea. Forecasting*, **21**, 689–714.
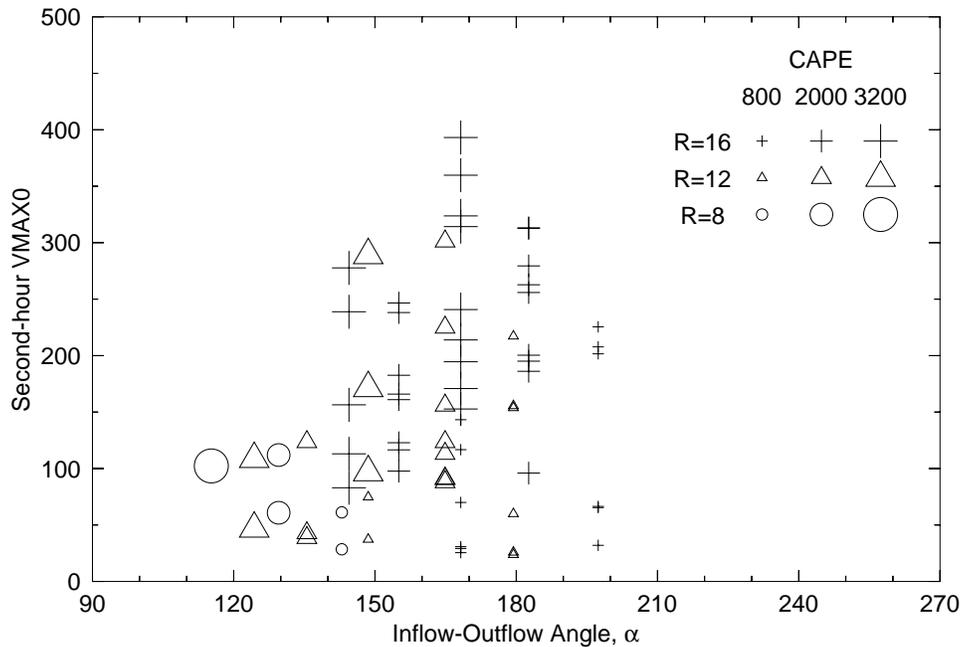
Fig. 6.   As in Fig. 5, but using the B2K storm motion forecast for the 72 simulated supercells.

Bunkers, M. J., B. A. Klimowski, J. W. Zeitler, R. L. Thompson, and M. L. Weisman, 2000: Predicting supercell motion using a new hodograph technique. *Wea. Forecasting*, **15**, 61–79.

Davies-Jones, R. P., D. Burgess, and M. Foster, 1990: Test of helicity as a tornado forecast parameter. *Preprints, 16th Conf. on Severe Local Storms*, 588–592, Kananaskis Park, AB, Canada, Amer. Meteor. Soc.

Droegemeier, K. K., S. M. Lazarus, and R. P. Davies-Jones, 1993: The influence of helicity on numerically simulated convective storms. *Mon. Wea. Rev.*, **121**, 2005–2029.

Kerr, B. W. and G. L. Darkow, 1996: Storm-relative winds and helicity in the tornadic thunderstorm environment. *Wea. Forecasting*, **11**, 489–505.

Kirkpatrick, C., E. W. McCaul, Jr., and C. Cohen, 2006: The influence of eight basic environmental parameters on the low-level rotation characteristics of simulated convective storms. *Preprints, 23rd Conf. on Severe Local Storms*, St. Louis, MO, Amer. Meteor. Soc., CD-ROM, 16.3.

Kirkpatrick, C., E. W. McCaul, Jr., and C. Cohen, 2007: The motion of simulated convective storms as a function of basic environmental parameters. *Mon. Wea. Rev.*, **135**, 3033–3051.

McCaul, E. W., Jr. and C. Cohen, 2002: The impact on simulated storm structure and intensity of variations in the mixed layer and moist layer depths. *Mon. Wea. Rev.*, **130**, 1722–1748.

McCaul, E. W., Jr., C. Cohen, and C. Kirkpatrick, 2005: The sensitivity of simulated storm structure, intensity, and precipitation efficiency to environmental temperature. *Mon. Wea. Rev.*, **133**, 3015–3037.

McCaul, E. W., Jr. and M. L. Weisman, 2001: The sensitivity of simulated supercell structure and intensity to variations in the shapes of environmental buoyancy and shear profiles. *Mon. Wea. Rev.*, **129**, 664–687.

Rasmussen, E. N. and D. O. Blanchard, 1998: A baseline climatology of sounding-derived supercell and tornado forecast parameters. *Wea. Forecasting*, **13**, 1148–1164.

Rasmussen, E. N. and J. M. Straka, 1998: Variations in supercell morphology. Part 1: Observations of the role of upper-level storm-relative flow. *Mon. Wea. Rev.*, **126**, 2406–2421.

Thompson, R. L., R. Edwards, J. A. Hart, K. L. Elmore, and P. Markowski, 2003: Close proximity soundings within supercell environments obtained from the Rapid Update Cycle. *Wea. Forecasting*, **18**, 1243–1261.

Thompson, R. L., C. M. Mead, and R. Edwards, 2007: Effective storm-relative helicity and bulk shear in supercell thunderstorm environments. *Wea. Forecasting*, **22**, 102–115.

Wakimoto, R. M. and J. W. Wilson, 1989: Non-supercell tornadoes. *Mon. Wea. Rev.*, **117**, 1113–1140.

Weisman, M. L. and J. B. Klemp, 1982: The dependence of numerically simulated convective storms on vertical wind shear and buoyancy. *Mon. Wea. Rev.*, **110**, 504–520.

Weisman, M. L. and J. B. Klemp, 1984: The structure and classification of numerically simulated convective storms in directionally varying shears. *Mon. Wea. Rev.*, **112**, 2479–2498.